PERGAMON

Vision Research 42 (2002) 589–597

Vision Research

www.elsevier.com/locate/visres

Symmetry perception: a novel approach for biological shapes ☆

Hugh R. Wilson *, Frances Wilkinson

Centre for Vision Research, 103 Farquharson, York University, 4700 Keele Street, Toronto, Ontario, Canada M3J 1P3

Received 23 April 2001; received in revised form 2 October 2001

Abstract

The majority of quantitative studies on symmetry perception have employed random dot patterns, yet symmetrical random patterns are not common in nature. Here we explore symmetry perception utilizing sums of radial frequency (RF) patterns to define complex shapes. When a pair of RF patterns with different frequencies are added, the relative phase of the two components provides a precise measure of the degree of deviation from bilateral symmetry. Sums of RF2–RF7 define such diverse biological shapes as human heads, animal heads, torsos, and many fruit, so discrimination of symmetries defined by these patterns is highly relevant to biological vision. Here we show that symmetry discrimination during brief presentations is best for RF2 + RF3 but becomes impossible for RF2 + RF7. Further experiments demonstrate that the underlying neural mechanisms differ from those involved in random dot symmetry detection. These results were used to predict symmetry thresholds for deviations from bilateral symmetry of head shapes based on a principal components analysis of 30 female heads. Human V4 is hypothesized to be the site for symmetry discrimination of RF patterns but not of random dot patterns.

Keywords: Symmetry; Random dots; Radial frequency; Head shape; V4; Principal components

1. Introduction

Ernst Mach (1959) used arrays of random shapes to demonstrate that only bilateral (and not, for example repetition or centric) symmetry is easily perceived. Following the elegant studies of Julesz (1971) much recent work on bilateral symmetry detection has employed random dot or random line patterns (see Tyler, 1996). Among the valuable results of these studies is the report that the symmetry of random dot patterns is conveyed only by dots close to the vertical symmetry axis (Dakin and Herbert, 1998; Gurnsey et al., 1998). For example, Dakin and Herbert (1998) showed that the spatial region for symmetry perception in bandpass filtered random dot patterns was restricted to an ellipsoid 3.5 cycles of the peak frequency wide and about 7.0 cycles high along the vertical symmetry axis. It should be noted, however, that Tyler and Hardage (1996) have produced data that question this result. Furthermore, it has been shown that the Dakin and Watt (1994) oriented spatial filtering model does a good job of predicting symmetry thresholds for filtered random dot patterns (Dakin and Hess, 1997). Thus, random dot symmetry studies suggest that bilateral symmetry information can be processed only near the symmetry axis. Furthermore, several studies have concluded that this symmetry axis must be centrally fixated for the information to be processed effectively (Gurnsey et al., 1998; Saarinen, 1988). Again, however, differing techniques have resulted in at least one study showing little eccentricity variation of bilateral random dot symmetry discrimination (Tyler, 1999).

Certainly, random dot-like patterns occur in nature, for example leaves or pebbled beaches viewed from a distance. However, these natural textures are seldom bilaterally symmetric, which leads to the question: Can the results of random dot symmetry studies be generalized to the large categories of biological shapes that are non-random but do possess (approximate) bilateral symmetry? Obvious examples of such shapes are human and animal heads in front view, torsos, and many fruits (pears, apples, oranges, etc.). There are several major reasons why bilateral symmetry of biological shapes is perceptually important. First, it has been demonstrated that finches and other animals will preferentially mate

☆ Portions of this research were first reported at the Annual Meeting of the Association for Research in Vision and Ophthalmology, May 1997.

* Corresponding author. Tel.: +1-416-736-2100.
E-mail address: hrwilson@yorku.ca (H.R. Wilson).

0042-6989/02/$ - see front matter
PII: S0042-6989(01)00299-1

with a visually symmetric partner (e.g. Swaddle and Cuthill, 1994). Also, studies of human facial attractiveness show that bilateral symmetry is a major determinant of perceived beauty (Langlois and Roggman, 1990; Scheib et al., 1999; Thornhill and Gangestad, 1993). This has been linked to mating preference through the observation that precise bilateral facial symmetry is developmentally difficult to generate and thus reflects a relative absence of genetic defects likely to distort symmetry. Secondly, we have recently shown that deviations from symmetry provide one major visual cue to the direction in which a person's head is pointing (Wilson et al., 2000). This is an obviously important social cue in inferring a person's focus of visual attention in social situations.

In this paper we present a novel approach to quantizing and measuring bilateral symmetry discrimination thresholds for head-like and other quasi-biological shapes. Our patterns are all constructed from sums of radial frequency (RF) patterns, which represent deviations from circularity to which humans are exquisitely sensitive (Wilkinson et al., 1998). Key to our stimulus design is the observation that sums of two or more RFs are only symmetric when the component frequencies have the correct relative phases in polar coordinates. For briefly flashed patterns, our data show that humans can only detect bilateral symmetry using RF components that are prominent in the mathematical description of human head shapes. Further experiments demonstrate that the underlying neural mechanisms have characteristics distinct from those involved in random dot symmetry tasks. Based upon recent fMRI (Wilkinson et al., 2000) and the effects of brain lesions (Gallant et al., 2000), we hypothesize that the locus of the underlying neural mechanisms is human V4.

2. Methods

All stimuli were presented on the screen of an iMac computer with 1024×768 resolution and temporal refresh rate of 75 Hz. Gray scale was linearized using custom software written by the authors. Subjects viewed the screen from 1.31 m away with their heads comfortably positioned in a chin rest. At this distance, each pixel subtended 47.1″ in diameter. A two temporal interval forced choice procedure was used with each trial initiated by the subject. Two patterns, one bilaterally symmetric and one not, were presented sequentially for 160 ms each to preclude multiple fixations. The method of constant stimuli was used with four progressively larger deviations from bilateral symmetry randomly presented.

All stimuli were defined by sums of RF patterns (Wilkinson et al., 1998; related patterns that were not bandpass filtered were used by Alter and Schwartz, 1988). In the main experiments just two RF patterns were summed, so the radius R as a function of angle θ in polar coordinates was defined by:

$$R(\theta) = R_0\left(1 + \sum_{n=1}^{2} A_n \cos\left(2\pi\omega_n\theta + \phi_n\right)\right) \quad (1)$$

where R_0 is the mean radius (0.5° in most experiments), A_n is the amplitude, ω_n the radial frequency (always an integer), and ϕ_n the phase. These RF patterns are made bandpass in spatial frequency by requiring the contour defined by Eq. (1) to have a fourth Gaussian derivative ($D4$) luminance profile centered on $R(\theta)$:

$$D4(r) = C\left\{1 - 4\left(\frac{r - R(\theta)}{\sigma}\right)^2 + \frac{4}{3}\left(\frac{r - R(\theta)}{\sigma}\right)^4\right\} \times \exp\left(-\left(\frac{r - R(\theta)}{\sigma}\right)^2\right) \quad (2)$$

where C is pattern contrast (100% in our experiments) and r is radius. The space constant σ was set to 0.056° in most experiments to make the peak spatial frequency 8.0 cpd. As our experiments were based on bilateral symmetry about an almost vertical axis (see below), we adopt the convention that the zero of the polar angle coordinate is vertically upwards, so when $\phi_n = 0°$ or 180° for every frequency n the pattern must be bilaterally symmetric about the vertical. When one frequency is even, a 90° phase shift of the other component will always produce a pattern that is bilaterally symmetric about a horizontal axis. For these patterns, therefore, the maximum deviation from bilateral symmetry about one or the other axis is represented by a relative phase shift of ±45° of the higher frequency component. Accordingly, only deviations up to ±45° from bilateral symmetry were used in our experiments.

Combinations of radial frequencies (RF2 + RF3), (RF2 + RF4), and (RF2 + RF5) are illustrated in Fig. 1 with bilateral symmetry about a vertical axis (left column) or with a phase rotation of 30° for the higher frequency component to produce a pattern lacking bilateral symmetry (right column). In these patterns the RF amplitudes were set to ten times mean detection thresholds reported previously (Wilkinson et al., 1998). Thus, $A_2 = 0.10$, $A_3 = 0.04$, and $A_n = 0.03$ for $n \geqslant 4$. It is evident from Fig. 1 that the asymmetric patterns have an apparent tilt of their long axis away from vertical, which might have provided an extraneous cue to asymmetry. Furthermore, even biological patterns possessing bilateral symmetry are seldom oriented so that the symmetry axis is exactly vertical. Indeed, measurements of two recent newspaper photographs of US president Dubya Bush indicated that in one his head, although pointing toward the camera, was tilted 5° to the left, while in the other it was tilted 7.5° to the right. In short, humans are frequently confronted with the visual task of detecting bilateral symmetry in patterns with a symmetry axis

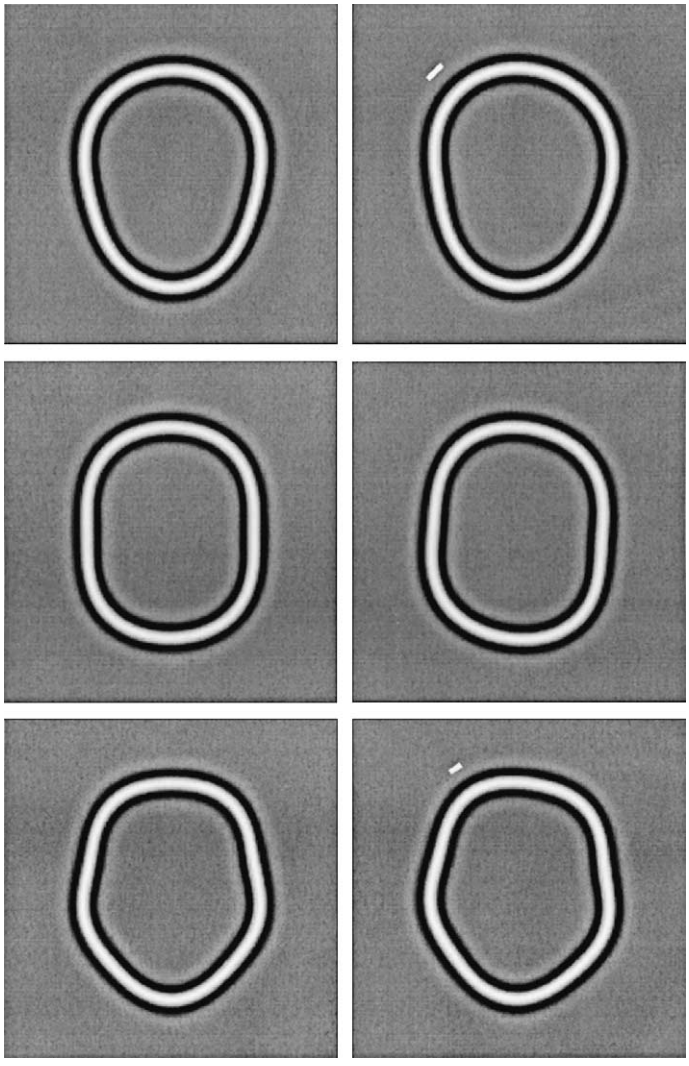

Fig. 1. Two component RF patterns. Patterns on the left have a vertical bilateral symmetry axis, while those on the right are not symmetric due to a phase rotation of the higher RF component by 30° relative to the lower. In all patterns the lower component was RF2, while the higher frequency component was (from top to bottom) RF3, RF4, and RF5. Component amplitudes were those used in the majority of experiments: 0.1 for RF2, 0.04 for RF3, and 0.03 for RF4 and RF5. Short white lines in top and bottom right panels (not present in experiments) illustrate the position shift of the local curvature maxima in these patterns relative to the symmetric case. Note that this shift is inversely proportional to frequency and therefore is larger for RF3 (top) than for RF5 (bottom).

near but not identical to vertical. Accordingly, we randomly rotated both the symmetric and asymmetric patterns in our experiments $\pm 6.0°$ left or right of vertical. Note that this is less than half the smallest orientation bandwidths ($\pm 15°$ at half amplitude) of psychophysically measured orientation-selective mechanisms (Wilson, 1991a).

A further point must be stressed concerning the effects of phase shifts to produce asymmetric patterns. Reference to Eq. (1) shows that a phase shift of any component represents a fraction of a cycle of that component. Relative to a 360° polar coordinate representation of the entire contour, therefore, the 30° phase shift of the RF3 component at the top right of Fig. 1 represents $30°/3 = 10°$ rotation of the points of maximum curvature around the circle. For the RF4 and RF5 components in the middle and bottom of Fig. 1, the equivalent rotations of maximum curvature loci are 7.5° and 6° respectively. These shifts are illustrated by short white lines in the top and bottom right panels. The importance of this point will become apparent from the experimental results.

In each two temporal interval forced choice experiment the subject's task on each trial was to pick the interval in which the asymmetric pattern had been presented. Four equally spaced phase shifts of the higher RF away from bilateral symmetry were randomly interspersed, with the maximum deviation always being $\leqslant 45°$ of phase for the reason indicated above. Using maximum likelihood estimation, data were fit with a

Quick (1974) or Weibull (1951) function to determine the 75% correct discrimination threshold. All experiments were repeated at least three times, so the means and standard errors of threshold measurements are reported.

Our final experiment was designed to relate our results from pairs of RFs to bilateral symmetry of an important biological shape: the human head. Accordingly, we took full-face digital photographs of 30 female volunteers and fit each with a sum of RF1–RF7. After correction for individual head size (i.e. normalization of RF amplitudes relative to mean head radius), amplitudes were averaged for each RF with the results shown in Fig. 2a. The dominant component is RF2 with a relative amplitude of 0.20 reflecting the average $(1+0.2)/(1-0.2)=1.5$ ratio of head height to width. Amplitudes of RFs above and below RF2 drop off fairly dramatically on a logarithmic scale. Chimpanzee skulls have likewise been reported to have a peak at RF2 and the largest amplitudes at frequencies below RF7 (O'Higgins, 1997). Mean phases for all RFs were very close to perfect bilateral symmetry, so a perfectly bilaterally symmetric average female head was produced by adjusting all phases to symmetry (phases are indicated in Fig. 2a). The bilaterally symmetric mean female head shape produced in this manner is illustrated in Fig. 2b. Historically, it is interesting to note that the first polar coordinate Fourier shape description was introduced to quantify human head shape (Lu, 1965).

To determine how deviations from bilateral symmetry are engendered in the human head, a principal components analysis was conducted using the phases of RF2–RF4 and RF5. This analysis omitted RF1 because of the extremely high threshold for detecting this frequency in patterns (Wilkinson et al., 1998), while RF6 and RF7 were excluded as a result of basic symmetry thresholds reported below in Fig. 3. This analysis revealed that the first principal component weighted the phases as follows: $0.0\phi_2+0.78\phi_3+0.83\phi_4-0.12\phi_5$. ($\phi_2$ presumably was weighted so minimally because of the dominant vertical elongation common among all heads.) Normalizing and rounding these factors, asymmetric head shapes were produced by rotating RF3 and

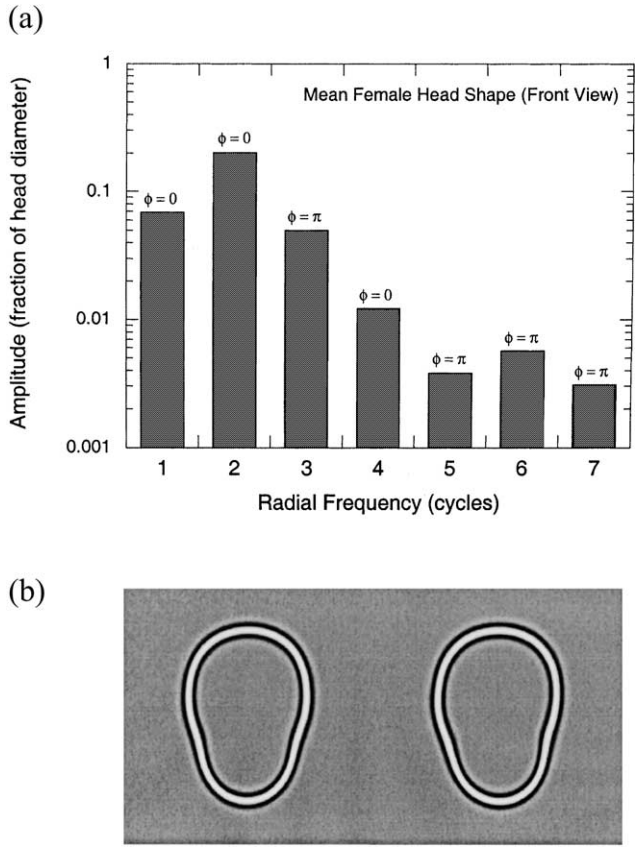

Fig. 2. Amplitudes and phases of RF components in a full face view of the female head produced by averaging photographs of 30 college-age volunteers. (a) RF amplitudes plotted as a fraction of head diameter show that RF2 is the dominant radial frequency, with both lower and higher RF amplitudes being significantly smaller on this logarithmic scale. The amplitude of RF7 is approximately at its own detection threshold (Wilkinson et al., 1998), and higher RFs are insignificant for describing head shapes. Similar amplitudes have been reported for side views of chimpanzee crania (O'Higgins, 1997). Phases for generating a head shape with perfect bilateral symmetry (representing minimal shifts from the average phases) are indicated by values of ϕ above the bars. (b) Bilaterally symmetric female head shape (left) and asymmetric head (right) produced by rotating the first principal component of RF phases through an angle of 18°, above the mean threshold for our subjects.

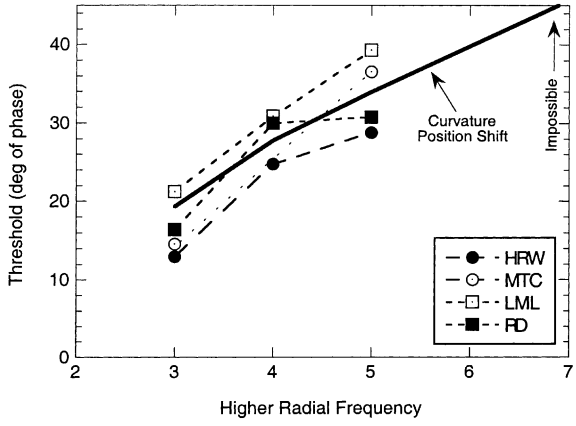

Fig. 3. Bilateral symmetry discrimination thresholds (quantified as degrees of phase rotation of the higher frequency component) for two-component RF patterns. The lower component was always RF2, while the higher was RF3–RF7 as indicated on the abscissa (see Fig. 1 for stimuli). Thresholds for all subjects increased roughly linearly from (RF2 + RF3) to (RF2 + RF5). All subjects were also tested with (RF2 + RF7), but symmetry discrimination with this combination was found to be impossible as subjects' performances were still only slightly above chance for a 45° phase rotation. The solid line shows thresholds predicted by a fixed shift in the position of maximum curvature, based on the measured mean threshold for RF4. In this and all subsequent graphs error bars are shown when larger than the plotting symbols and represent standard errors of the mean.

RF4 through the same positive phase angle ϕ_{rot} while rotating RF5 in through $-0.15\phi_{rot}$. Phases of RF1, RF2, RF6, and RF7 remained at their symmetric phases. Heads with various degrees of asymmetry were produced by varying ϕ_{rot}, and an example where $\phi_{rot} = 18°$ is shown in the right in Fig. 2b. In experiments these head shapes were randomly rotated by ±6° as described above for two component patterns.

3. Basic results

Our basic experiments measured bilateral symmetry discrimination thresholds for two component RF patterns containing RF2 plus one higher frequency (RF3–RF7). Results for patterns with mean radius $R_0 = 0.5°$ (Eq. (1)), plotted in Fig. 3 for four subjects, show that thresholds are lowest for the (RF2 + RF3) combination and rise progressively for RF2 combined with RF4 or RF5. Thresholds averaged across subjects were 16.5°, 28.6°, and 34.0° for combinations with higher component RF3–RF5 respectively. Experiments using the combination (RF2 + RF7) were run on all subjects, but in every case discrimination had not reached threshold for a 45° phase shift of the RF7 component. As greater phase shifts in this case lead toward a more symmetric pattern about the horizontal axis, bilateral symmetry discrimination is impossible for the (RF2 + RF7) combination. This conclusion, of course, is dependent on our use of a brief 160 ms presentation plus randomization of the symmetry axis orientation by ±6°. The solid line in Fig. 1 reflects a constant shift of the loci of maximum curvature (see Section 2) and provides a good description of the trend in the data (see Section 5 for details).

It is possible that the visual system can only extract symmetry information from patterns containing RF components of closer frequencies than RF2 and RF7. To assess this possibility, two subjects were run on the combinations (RF3 + RF5) and (RF5 + RF7). Symmetry thresholds averaged 31.1° for the former and 39.8° for the latter combination. Thus, RF7 can be used by the visual system for discrimination of bilateral symmetry in this combination, but the thresholds are higher than for either (RF3 + RF5) or (RF2 + RF4) (mean 28.6° in Fig. 3). This suggests that the visual system is strongly biased towards lower radial frequencies in symmetry discrimination.

As thresholds were lowest for the (RF2 + RF3) combination, additional experiments were conducted with this pattern. The effects of doubling the pattern radius to $R_0 = 1.0°$ while keeping the peak spatial frequency constant at 8.0 cpd are plotted in Fig. 4. It is evident that thresholds for 1.0° radius patterns always fell within 1.0 standard error of 0.5° radius thresholds. Thus, bilateral symmetry discrimination with these

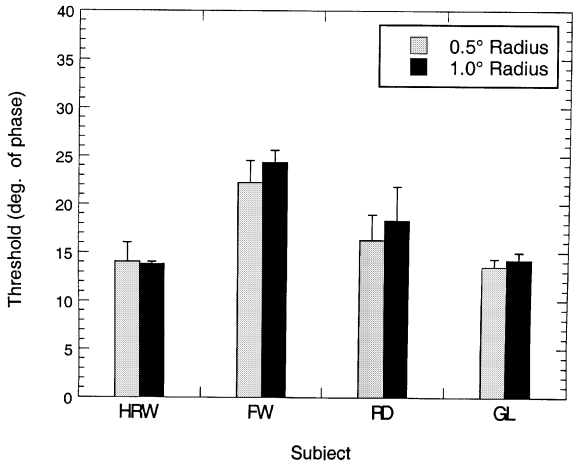

Fig. 4. Comparison of symmetry thresholds for the (RF2 + RF3) combination with mean radius of 0.5° (grey bars) and 1.0° (black bars). For both patterns the spatial frequency remained constant at 8.0 cpd. For all subjects the two pattern sizes produced symmetry thresholds within one standard error of each other, thus indicating size constancy for bilateral symmetry perception.

patterns exhibits almost perfect size constancy over a twofold size variation. Wilkinson et al. (1998) also reported size constancy for detection of RF patterns over a wide size and spatial frequency range.

A further question of interest is whether the amplitudes of the RF components affect symmetry thresholds. It is obvious that as component amplitudes drop near threshold, producing a more nearly circular pattern, symmetry thresholds must rise until the task ultimately becomes impossible. The more interesting question, therefore, is whether *larger* RF amplitudes will *decrease* thresholds further. To test this possibility, bilateral symmetry thresholds were re-measured for the (RF2 + RF3) pattern with both component amplitudes doubled to 0.2 and 0.08 respectively. Bilateral symmetry thresholds for these patterns are plotted in Fig. 5. There is evidently no major improvement in discrimination with the larger RF component amplitudes (black bars) relative to the lower amplitude (gray bars): for three subjects thresholds fall within one standard error of one another, while the last (MTC) actually performed more poorly with the higher amplitudes. Thus it appears that bilateral symmetry discrimination thresholds have reached an asymptote when the component RF amplitudes are at least ten times threshold (gray bars).

In order to determine whether bilateral symmetry discrimination was possible in the visual periphery, thresholds were measured for the (RF2 + RF3) pattern centered at 8.0° eccentricity along the horizontal axis. Relative to the 0.5° radius, 8.0 cpd foveal stimulus, the peripheral stimulus was scaled by a factor of 3.0 to a radius of 1.5° and spatial frequency of 2.67 cpd to compensate for the difference in local acuity. Data for two subjects are plotted in Fig. 6. The peripheral

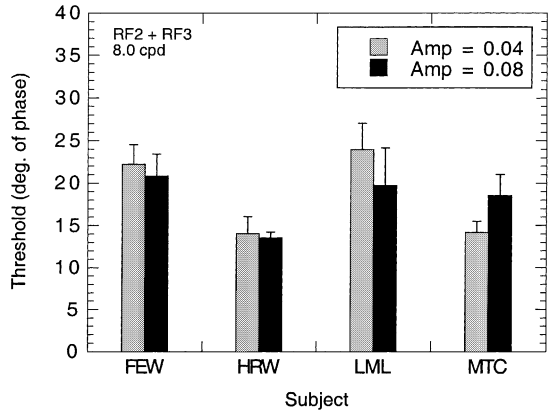

Fig. 5. Effect of RF amplitudes on bilateral symmetry thresholds for (RF2 + RF3). Grey bars show data for the base condition with amplitudes of 0.1 and 0.04 for RF2 and RF3 respectively (ten times detection threshold for each, Wilkinson et al., 1998), while black bars plot data for RF patterns with amplitudes doubled to 0.2 and 0.08 respectively. Increasing RF component amplitude had no systematic effect on thresholds.

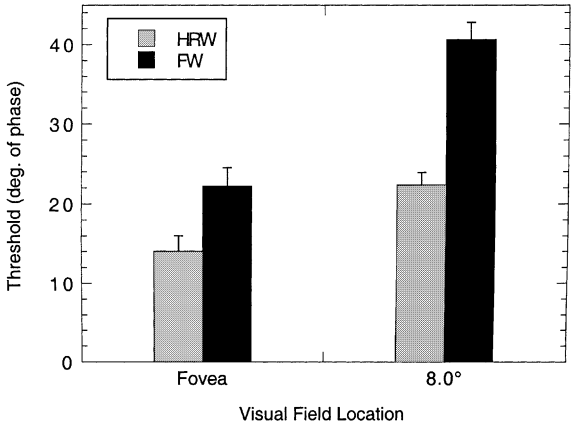

Fig. 6. Symmetry thresholds for the (RF2 + RF3) combination centered at 8.0° eccentricity compared to foveal thresholds. The foveal pattern had a mean radius of 0.5° and spatial frequency of 8.0 cpd, while the peripheral pattern was scaled to 1.5° radius and 2.67 cpd peak spatial frequency. Although thresholds for both subjects were elevated in the periphery, bilateral symmetry discrimination is still possible at 8.0° eccentricity.

threshold was 1.6 times higher than in the fovea for HRW and 1.8 times higher for FEW. Nevertheless, bilateral symmetry discrimination, although degraded, was still possible at this eccentricity.

Bilateral symmetry perception in bandpass random dot patterns has been reported to require information in a spatial band about 3.5 cycles of the spatial period in width centered upon the symmetry axis (Dakin and Herbert, 1998). If such were also the case for RF patterns, then elimination of a band of contour about the symmetry axis should make discrimination difficult or impossible. Accordingly, a 0.625° wide band (5.0 cycles of 8.0 cpd) was replaced by the mean luminance in a 1.0°

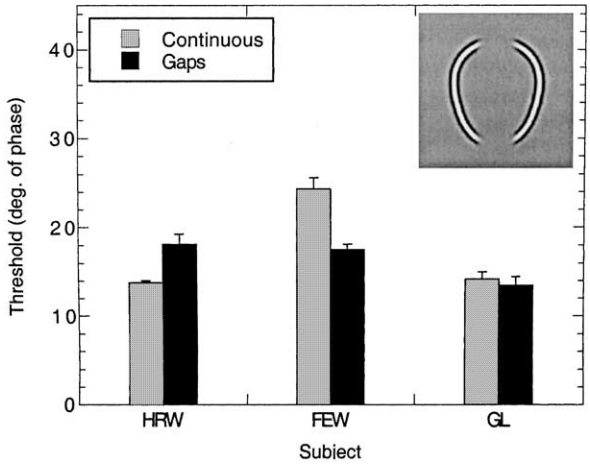

Fig. 7. Effects of a 5.0 cycle wide gap centered on the symmetry axis in the (RF2 + RF3) symmetry pattern (see insert). Patterns had a peak spatial frequency of 8.0 cpd and a mean radius of 1.0°. Relative to patterns without gaps (grey bars), thresholds for gap patterns (black bars) produced a modest performance decrement for HRW, a performance improvement for FEW, and no statistically significant change for GL. Overall, therefore, removal of all information within the 5.0 cycle wide gap produced no consistent change in bilateral symmetry thresholds.

radius (RF2 + RF3) pattern, as depicted by the inset in Fig. 7. The edges of these contour gaps were smoothed by a narrow Gaussian to eliminate any aliasing artifacts when the patterns were presented at ±6° orientations in the experiments. The data in Fig. 7 reveal that all subjects could readily discriminate bilateral symmetry in these patterns. There was some individual variation, as FEW improved slightly with the gaps pattern, HRW became slightly worse, while GL remained essentially unchanged. Thus, contour information within ±2.5 cycles of the symmetry axis is not necessary and has no consistent effect on symmetry discrimination for RF patterns when averaged across subjects.

Two ancillary experiments were conducted on two subjects using the (RF2 + RF3) combination. First, symmetry measurements were repeated with the symmetry axis oriented at 45° to vertical, a manipulation that produced a 52% increase in thresholds. Thus, there is an oblique effect for RF symmetry discrimination. Second, the phase of the RF2 component was rotated 180° relative to the RF3 component. This produced a pattern with a vertical symmetry axis but a horizontal elongation as opposed to the patterns in Fig. 1 where both elongation and symmetry axes are vertical. Thresholds increased an average of 30% for discrimination of bilateral symmetry about a vertical axis in such horizontally elongated patterns.

All symmetry thresholds reported above were measured under conditions where each pattern was presented with its symmetry axis randomly oriented at ±6° relative to the vertical. As discussed above, this manipulation is reasonable given that bilaterally symmetric

objects are seldom exactly vertical under real viewing conditions. Nevertheless, it is of interest to determine whether thresholds improve when the ±6° orientation jitter is eliminated. Accordingly, thresholds were re-measured on two subjects with a fixed vertical pattern presentation, and this improved thresholds by an average of 25%. Thus, the requirement that the visual system compute orientation of the potential symmetry axis in addition to assessing symmetry engenders a modest performance penalty, at least for 160 ms stimulus presentations.

4. Symmetry of human heads

The experiments reported above establish that thresholds for bilateral symmetry discrimination can be readily measured for two component RF patterns, at least when both frequencies are below RF7. Can these results be related to symmetry discrimination using biologically important images such as human heads? This was tested using a mean female head shape synthesized out of RF1–RF7 using the data in Fig. 2 (see Section 2). As the first principal component of head symmetry variation in our population involved equal phase rotations ϕ of RF3 and RF4 relative to RF2 but an opposite rotation of RF5 by -0.15ϕ, symmetry thresholds were measured by varying this principal component. Phases of all other components remained in bilateral symmetry phase. Based on the data in Fig. 3 on two component RF patterns, we predicted that the common rotation of RF3 and RF4 would at least partially summate to compensate for the rather minor negative contribution of RF5 and produce thresholds lower than for any two component RF pattern in Fig. 3. Symmetry thresholds for the head shape are compared with the (RF2 + RF3) threshold for three subjects in Fig. 8. All three subjects had lower phase thresholds for discriminating symmetry of head shapes than for the (RF2 + RF3) combination, and this difference was statistically significant across subjects ($t_2 = 7.35$, $p < 0.02$). Thus, the qualitative prediction based on the data in Fig. 3 is supported by symmetry discrimination of mean female head shapes.

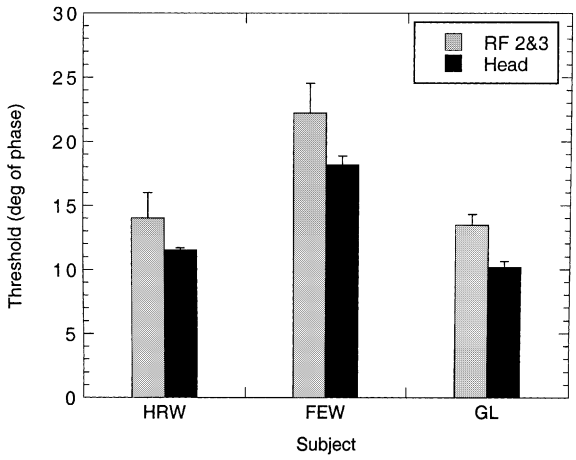

Fig. 8. Symmetry thresholds for the (RF2 + RF3) combination (grey bars) compared to a mean female head shape synthesized from RF1–RF7 (see Fig. 2b). As described in the text, thresholds for the head were determined by rotating the first principal component of the phase variation in our population of 30 female heads. For all subjects thresholds were significantly lower for the head shape than for the two component RF pattern, thus indicating partial summation between component rotations in the first principal component (see text).

5. Discussion

These experiments establish that bilateral symmetry thresholds can be measured quantitatively for biologically significant shapes using component phase shifts in RF patterns. Furthermore, symmetry data from two component RF patterns suffice to qualitatively predict thresholds for human head symmetry based on principal component analysis. Our data also suggest that the most relevant radial frequencies for bilateral symmetry perception fall within the RF2–RF6 range: RF7 supported little or no symmetry discrimination, while RF1 has an amplitude detection threshold over 20 times higher than other radial frequencies (Wilkinson et al., 1998). It is significant that this RF2–RF6 range represents most of the variance of human (see Fig. 2a) and chimpanzee head shapes (O'Higgins, 1997) and that these radial frequencies can be very accurately identified even with short presentations near threshold (Wilkinson et al., 1998). Furthermore, RF symmetry discrimination exhibits size constancy (see Fig. 4) as does RF detection (Wilkinson et al., 1998).

As phase rotation of the higher radial frequency is a novel metric, it is instructive to recalculate symmetry discrimination thresholds in more conventional units. In a bilaterally symmetric pattern, points mirrored on opposite sides of the symmetry axis lie at the same distance from that axis. Calculation shows that the 16.5° mean phase threshold for the (RF2 + RF3) pattern entails a maximum shift in positioning of such mirror points by 40.0″ (0.011°) for points separated by 0.9°. This threshold is almost two times smaller than the 72.0″ (0.02°) threshold for two line separation discrimination at a base separation of 1.0° reported by Levi et al. (1988). Furthermore, these discrimination thresholds are near the theoretical limit imposed by irregularity in cone spacing outside the fovea (Wilson, 1991b). Clearly, therefore, the lowest symmetry discrimination thresholds for RF combinations fall within the hyperacuity range for distance comparisons at a 0.9–1.0° separation.

Insight into the cues subjects may be using for symmetry discrimination of RF patterns is provided by the data in Fig. 3. Thresholds described in degrees of phase rotation clearly rise almost linearly with the frequency of

the higher RF component. As indicated in Section 2, the effect of a fixed phase rotation is to shift the locations of curvature extrema by a distance that is inversely proportional to pattern radial frequency. Consider the hypothesis that symmetry thresholds are determined by a fixed shift in the positions of curvature extrema, which would then correspond to a progressively larger phase shift for higher component RFs. The solid line in Fig. 3 shows thresholds predicted by such a constant curvature position shift, with the position of the line determined by the threshold for (RF2 + RF4). (The slightly steeper portion of this line between RF3 and RF4 results from the slightly higher amplitude of RF3 to keep it at ten times threshold.) This line provides a reasonable fit to the data, and its extrapolation to RF7 correctly predicts that the threshold should be above 45° of phase and therefore unmeasurable. This suggests that the visual system bases RF symmetry discrimination on assessment of the location of a potential symmetry axis based on pattern elongation (RF2) followed by global assessment of curvature extrema locations around the contour.

Our data suggest that distinct visual mechanisms analyze bilateral symmetry in RF patterns and biological shapes as opposed to random dot patterns. First, bilateral symmetry perception in random dot patterns becomes much more difficult (Saarinen, 1988) or impossible beyond an eccentricity of 3.8° (Gurnsey et al., 1998). In contrast, perception of symmetry in RF patterns is possible at least out to 8.0° eccentricity, although peripheral is poorer than foveal performance (see Fig. 6). Second, Dakin and Herbert (1998) have used bandpass filtered random dot patterns to show that the information used in bilateral symmetry perception is confined to a strip 3.5 cycles wide centered on the vertical symmetry axis. When a strip of contour 5.0 cycles wide is removed about the symmetry axis in a RF pattern, however, performance averaged across subjects is not changed significantly (see Fig. 7). Finally, models that have been quite successful in accounting for bilateral symmetry perception in random dot patterns (Dakin and Hess, 1997; Dakin and Watt, 1994) would not respond effectively to the bandpass contours and curvature extrema in RF symmetry patterns, because these models use only horizontally oriented filters to detect vertical symmetry. Such horizontally oriented filters will not respond to most of the RF contour in our patterns, which is bandpass filtered and deviates substantially from horizontal.

Taken together, these results all point to the presence of two different symmetry detection mechanisms in human vision. The first is involved in processing the symmetry of textured surfaces exemplified by random dot patterns, and plausible models of the underlying neural mechanisms have been suggested (Dakin and Hess, 1997; Dakin and Watt, 1994). Based upon our data, a second bilateral symmetry mechanism is optimized for processing the symmetric contours defining many biological shapes. Although we have not yet developed a detailed neural mechanism for RF contour symmetry perception, a first approach has been made using model V4 concentric units (Wilson et al., 1997). In particular, it has been shown that a population code based on model V4 concentric units does provide information about the increasing asymmetry of human head shapes as they are rotated away from a fronto-parallel view (Wilson et al., 2000). As this model is based upon global summation of concentric curvature information (Wilson et al., 1997), it also has the appropriate characteristics to record positions of local curvature extrema.

Given this evidence for the existence of separate symmetry mechanisms for textured surfaces and biological shapes, it is natural to conjecture that the underlying neural mechanisms may reside in different cortical areas. Although much work remains, two studies provide initial support for this possibility. An fMRI study by Tyler and Baseler (1998) showed that the middle occipital gyrus (MOG) responded more strongly to symmetric random dot patterns than to dot patterns without symmetry. In contrast, Wilkinson et al. (2000) showed that concentric, RF3 and RF5 patterns produced strong fMRI activation of human V4 and that these patterns also significantly activated the fusiform face area. (Human V4 was defined by location of the vertical meridian representations in cortex using flashing windmill wedges, Engel et al. (1997). Furthermore, damage to human V4 significantly disrupts discrimination of RF patterns (Gallant et al., 2000). This suggests that human V4 may contribute to symmetry analysis of RF patterns constitutive of biological shapes, while MOG may be specialized for symmetry of textured surfaces.

Radial frequencies below RF7 are readily identifiable in 160 ms presentations (Wilkinson et al., 1998), mediate the most precise symmetry discrimination (Fig. 3), and accurately describe human head shapes (Fig. 2). The phase rotation technique represents a novel measure of bilateral symmetry discrimination for many biological shapes synthesized from these RF components. The technique is more general, however, as introduction of increasing phase rotations over time has been used to study motion deformation in composite RF patterns (Loffler and Wilson, 2001). Thus, multi-component RF patterns should provide a rich psychophysical and physiological stimulus set for future explorations of symmetry and other aspects of biological shape perception.

Acknowledgements

This research was supported in part by NSERC grants #OPG227224 to HRW and #OPG0007551 to FW.

References

Alter, I., & Schwartz, E. L. (1988). Psychophysical studies of shape with Fourier descriptor stimuli. *Perception*, 191–202.

Dakin, S. C., & Herbert, A. M. (1998). The spatial region of integration for visual symmetry detection. *Proceedings of the Royal Society of London, Series B*, *265*, 659–664.

Dakin, S. C., & Hess, R. F. (1997). The spatial mechanisms mediating symmetry perception. *Vision Research*, *37*, 2915–2930.

Dakin, S. C., & Watt, R. J. (1994). Detection of bilateral symmetry using spatial filters. *Spatial Vision*, *8*, 393–413.

Engel, S. A., Glover, G. H., & Wandell, B. A. (1997). Retinotopic organization in human visual cortex and the spatial precision of functional MRI. *Cerebral Cortex*, *7*, 181–192.

Gallant, J. L., Shoup, R. E., & Mazer, J. A. (2000). A human extrastriate cortical area that is functionally homologous to macaque area V4. *Neuron*, *27*, 227–235.

Gurnsey, R., Herbert, A. M., & Kenemy, J. (1998). Bilateral symmetry embedded in noise is detected accurately only at fixation. *Vision Research*, *38*, 3795–3803.

Julesz, B. (1971). *Foundations of Cyclopean Perception*. Chicago: University of Chicago.

Langlois, J. H., & Roggman, L. A. (1990). Attractive faces are only average. *Psychological Science*, *1*, 115–121.

Levi, D. M., Klein, S. A., & Yap, Y. L. (1988). ''Weber's law'' for position: unconfounding the role of separation and eccentricity. *Vision Research*, *28*, 597–603.

Loffler, G., & Wilson, H. R. (2001). Detecting shape deformation of moving patterns. *Vision Research*, *41*, 991–1006.

Lu, K. H. (1965). Harmonic analysis of the human face. *Biometrics*, *21*, 491–505.

Mach, E. (1959). *The analysis of sensations* (C. M. Williams, Trans.). New York: Dover Publications (Original work published 1886).

O'Higgins, P. (1997). Methodological issues in the description of forms. In: P. E. Lestrel (Ed.), *Fourier descriptors and their applications in biology* (pp. 74–105). Cambridge: Cambridge University Press.

Quick, R. F. (1974). A vector-magnitude model of contrast detection. *Kybernetik*, *16*, 1299–1302.

Saarinen, J. (1988). Detection of mirror symmetry in random dot patterns at different eccentricities. *Vision Research*, *28*, 755–759.

Scheib, J. E., Gangestad, S. W., & Thornhill, R. (1999). Facial attractiveness, symmetry and cues of good genes. *Proceedings of the Royal Society of London, Series B*, *266*, 1913–1917.

Swaddle, J. P., & Cuthill, I. C. (1994). Preference for symmetric males by female zebra finches. *Nature*, *367*, 165–166.

Thornhill, R., & Gangestad, S. W. (1993). Human facial beauty: averageness, symmetry, and parasite resistance. *Human Nature*, *4*, 237–269.

Tyler, C. W. (1996). *Human Symmetry Perception*. Utrecht: VSP.

Tyler, C. W. (1999). Human symmetry detection exhibits reverse eccentricity scaling. *Vision Neuroscience*, *16*, 919–922.

Tyler, C. W., & Baseler, H. A. (1998). Properties of the middle occipital gyrus: an fMRI study. *Society of Neuroscience Abstracts*, *24*, 594.7.

Tyler, C.W., & Hardage, L. (1996). Mirror symmetry detection: predominance of second-order pattern processing throughout the visual field. In: C. W. Tyler (Ed.), *Human Symmetry Perception* (pp. 157–171). Utrecht: VSP.

Weibull, W. A. (1951). A statistical distribution function of wide applicability. *Journal of Applied Mechanics*, *18*, 292–297.

Wilkinson, F., James, T. W., Wilson, H. R., Gati, J. S., Menon, R. S., & Goodale, M. A. (2000). An fMRI study of the selective activation of human extrastriate form vision areas by radial and concentric gratings. *Current Biology*, *10*, 1455–1458.

Wilkinson, F., Wilson, H. R., & Habak, C. (1998). Detection and recognition of radial frequency patterns. *Vision Research*, *38*, 3555–3568.

Wilson, H.R. (1991a). Psychophysical models of spatial vision and hyperacuity. In: D. Regan (Ed.), *Spatial Vision* (pp. 64–86). London: MacMillan.

Wilson, H.R. (1991b). Pattern discrimination, visual filters, and spatial sampling irregularity. In: M. Landy, & J. A. Movshon (Eds.), *Computational Models of Visual Processing* (pp. 153–168). Cambridge, MIT Press.

Wilson, H. R., Wilkinson, F., & Asaad, W. (1997). Concentric orientation summation in human form vision. *Vision Research*, *37*, 2325–2330.

Wilson, H. R., Wilkinson, F., Lin, L.-M., & Castillo, M. (2000). Perception of head orientation. *Vision Research*, *40*, 459–472.